Supplemental Material:
Terahertz Field Control of Electronic-Ferroelectric Anisotropy at Room Temperature in $LuFe_2O_4$

Hirotake Itoh,[1,*] Ryusei Minakami,[1] Hongwu Yu,[2] Ryohei Tsuruoka,[1] Tatsuya Amano,[1] Yohei Kawakami,[1] Shin-ya Koshihara,[2] Kosuke Fujiwara,[3,†] Naoshi Ikeda,[3] Yoichi Okimoto,[2,‡] and Shinichiro Iwai[1,§]

[1]*Department of Physics, Tohoku University, Sendai 980-8578, Japan*
[2]*Department of Chemistry, Institute of Science Tokyo, Tokyo 152-8551, Japan*
[3]*Graduate School of Natural Science and Technology, Okayama University, Okayama 700-8530, Japan*

(Dated: July 29, 2025)

(1) AN OVERVIEW OF RESEARCH ON RFe$_2$O$_4$

Below, we briefly outline the history of research on the ferroelectricity in RFe$_2$O$_4$ (R = Lu, Yb, Y, etc.). Note that several review papers have been already published[1–4].

RFe$_2$O$_4$ was first synthesized in the 1970s[5–8] triggering studies on its magnetism arising from spin frustration on a triangular lattice, which interestingly couples to transport property like that of a magnetite[9]. In the 1980s, the coexistence of Fe ions with different valences, in other words, charge ordering (CO), was indicated by Mössbauer study[10, 11] followed by diffraction experiments (neutron, electron beam, and x-ray) [12–14]. The CO or correlated charges therein was found to show anomalous dielectric behaviors in the 1990s[15, 16], opening an avenue to the electronic ferroelectricity reported in the 2000s[17, 18].

Motivated by this CO-induced peculiar polarization which may accompany multiferroicity[19], a number of experiments on its ferroelectricity including magnetoelectric effects[20–34], field-induced effects[35–50], optical properties[51–60], and theoretical studies[61–70] were carried out in the 2000s and the 2010s. Meanwhile, several reports have cast doubt upon the scenario of the electronic ferroelectricity[2, 27–31, 52], based on experimental observations of the CO without polar signature.

The controversial claims on macroscopic properties likely arose from the sensitive nature of a crystal to chemical nonstoichiometry (namely oxygen[31, 71–74] and iron[75] vacancies) and/or grain boundaries of polycrystalline samples[27, 76], because the concomitant disorder would unpredictably affect long-range order. Therefore, a high-quality stoichiometric single crystal is indispensable to validate the macroscopic phenomena.

In the late 2010s, the CO having long-range coherence was established using the crystals with not only oxygen[74] but also iron[75, 77] stoichiometry. Accordingly the improved crystal clearly exhibited reversible polarization current[78], while belonged to Laue class of 2/m[79] being consistent with previous studies[29, 31, 80]. In the 2020s macroscopic breaking of spatial inversion symmetry was unambiguously identified by optical second harmonic generation (SHG) experiment[81] which is undisturbed by electrodes[76]. By utilizing the phenomena, the ultrafast and sensitive nature of the electronic ferroelectricity is being investigated[82, 83] as described and presented in the main text. Ferroelectric polarization switching has also been confirmed by scanning probe techniques[84].

(2) THE EXPERIMENTAL SETUP

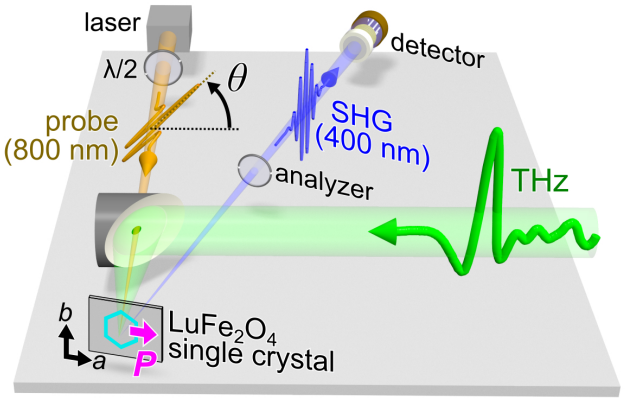

FIG. S1. Experimental setup.

Figure S1 shows schematics of the used experimental setup. The 800 nm-fundamental light was introduced onto the $LuFe_2O_4$ single crystal (ab-plane) and the resultant SHG intensity I_{SH} was measured in reflection geometry. Its anisotropy was characterized by fundamental polarization angle θ (θ = 0° corresponds to the a-axis) set by a $\lambda/2$ plate, namely, polarizer. The polarization angle of SHG ($\|b$ or a) was chosen by a polarization filter, namely, analyzer.

A bulk $LuFe_2O_4$ single crystal was synthesized using the floating melting method with special care on the stoichiometry [81]. The crystals have typical sizes of 3×3×2 mm^3. A cleaved ab-plane was used for the optical experiments, wherein the projected $\boldsymbol{P}$ orients to the a-axis [Figs. S1 and 1][81].

A 1-kHz Ti:sapphire regenerative amplifier system (Legend USX, Coherent Corp.) was used as a light source, and the output at 1.55 eV with a pulse width of 25 fs was divided into 2 beams. One was used to generate the terahertz light using a $LiNbO_3$ crystal and tilted-pulse-front technique[85, 86]. The collimated terahertz wave was focused on the sample using the parabolic mirror (MPD229H-M01, Thorlabs, Inc.).

A pair of wire-grid polarizers (GS57202, Specac Ltd.) was used to attenuate its electric field amplitude while maintaining the waveform. Its time-domain waveform was characterized by electro-optic sampling using a 0.4 mm-thick (110) GaP crystal and a balanced photodetector (Nirvana 2017, NewFocus, Inc.). The other beam, namely, the fundamental beam for the SHG, was focused to a spot of 300 μm ($1/e^2$ diameter) to be superimposed with the terahertz beam. Its fluence was 0.6 mJ/cm^2, which is in the regime where SHG shows a quadratic increase as expected. SHG was detected by a photomultiplier (H11461P-01, Hamamatsu Photonics K. K.) attached to a monochromator (M10, Bunkoukeiki Co., Ltd.) after high-pass filters. The polarization of the fundamental and the SHG were chosen by a $\lambda/2$ plate (WPQW-NIR-2M, SIGMAKOKI Co., Ltd.) and a wire-grid polarization filter (WP25M-UB, Thorlabs, Inc.), respectively. The SHG measurement scheme is essentially the same as that previously used [81].

The penetration depths of the fundamental and the SHG light is $l_{\rm fund} \simeq 190$ nm and $l_{\rm SH} \simeq 100$ nm, respectively[83]. The coherence length l_c of the SHG is 1.8 μm, which is estimated as $l_c = 2/|\Delta k| = \lambda/2\pi|\Delta n|$[87] where λ is the fundamental wavelength and Δn is the difference between the refractive indices of the fundamental and the SHG lights. Because $l_c \gg l_{\rm SH}$, the phase mismatch effect is negligibly small. The penetration depth for the used ≈1 terahertz pump light is $l_{\rm THz}$≃100 μm[58]; $l_{\rm THz} \gg l_{\rm SH}$ indicates that the region probed by the SHG is homogeneously pumped. The propagation time of the lights in the crystal is of the order of 1 fs as estimated by nl/c where c is the speed of light in vacuum and $n \approx 2$ is the refractive index of the used lights, therefore does not affect the observed dynamics on the subpicosecond timescale.

We have carefully designed the pump-probe setup to avoid the degradation in temporal resolution arising from poor spatial overwraps. The optic axes of the terahertz pump pulse (wavelength: $\lambda \approx 300\,\mu$m) and the probe fundamental pulse ($\lambda \approx 800$ nm) are colinear on the sample [Fig. S1](or the EO crystal used to characterize the terahertz waveform) hence the angle between them is zero. Both beams are focused on the sample, so their wavefronts should be planar therein. Considering the spot diameter of the probe beam (300 μm, smaller than that for the pump) and the angle to the surface normal (18.2°), the side edges of the probe beam reach the sample at 50 μm ($\approx \frac{300}{2}\,\mu$m $\times \sin 18.2°$) forward or backward compared to the center of the beam. Since this is much less than Rayleigh length of the beams ($\approx 1400\,\mu$m for the terahertz pump and $\approx 37000\,\mu$m for the probe as estimated by $\frac{\pi}{\lambda}\left(\frac{0.61\lambda}{\rm NA}\right)^2$), the shift from the focal point should be insignificant.

(3) SHG ANISOTROPY AND CONVERSION EFFICIENCY IN THE STEADY-STATE

Figure S2 shows intensities of SHG, $I_{\rm SH}(\theta)$, from the ab-plane of steady-state $LuFe_2O_4$ at room temperature. θ represents an azimuthal angle (from the a-axis) of the polarization of incident light [Fig. S1]: $(E_a, E_b) \propto (\cos\theta, \sin\theta)$. As shown, the amplitudes of $I_{{\rm SH}\|b}$ and $I_{{\rm SH}\|a}$ are comparable, similar to those for $YbFe_2O_4$ [81]. Their anisotropies are consistent with C_m point symmetry having an ac mirror plane (i.e., $\boldsymbol{P}$ in the ac-plane [Fig. 1]), as described below. 2nd-order nonlinear susceptibility tensor d_{ij} is expressed as

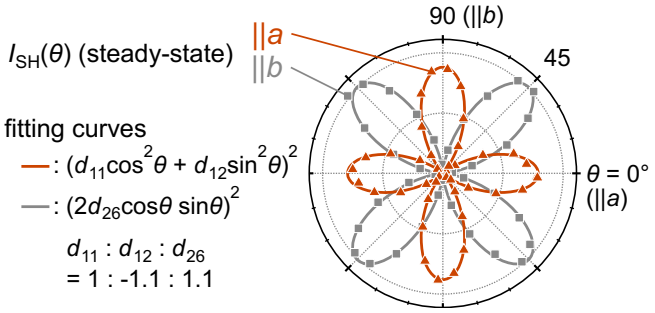

FIG. S2. $I_{\rm SH}(\theta)$ of steady-state $LuFe_2O_4$. $I_{\rm SH}\|a$ (brown triangle), $I_{\rm SH}\|b$ (grey square) and their fitting curves (solid lines) are shown.

$$d = \begin{pmatrix} d_{11} & d_{12} & d_{13} & 0 & d_{15} & 0 \\ 0 & 0 & 0 & d_{24} & 0 & d_{26} \\ d_{31} & d_{32} & d_{33} & 0 & d_{35} & 0 \end{pmatrix}, \tag{S1}$$

thereby $I_{\rm SH}$ being

$$I_{{\rm SH}\|a} = (d_{11}\cos^2\theta + d_{12}\sin^2\theta)^2 \tag{S2}$$

$$I_{{\rm SH}\|b} = (d_{26}\sin\theta\cos\theta)^2, \tag{S3}$$

by taking unessential coefficients as unity for simplicity. As expected, the observed $I_{{\rm SH}\|b}$ (grey square) shows the leaves-like 4-fold symmetry, and $I_{{\rm SH}\|a}$ (brown triangle) the cross-like shape. Accordingly, their fitting curves showed excellent overwrap yielding the result $d_{11} : d_{12} : d_{26} = 1 : -1.1 : 1.1$ close to that for $YbFe_2O_4$, $d_{11} : d_{12} : d_{26} = 1 : -1.1 : 1.2$ [81].

To characterize the absolute value for d or conversion efficiency, we have measured the SHG from the popular electro-optic material ZnTe as a benchmark, then compared that of $LuFe_2O_4$. Although ZnTe is transparent at the fundamental wavelength 800 nm, it is opaque at the SH wavelength 400 nm; the penetration depth $l_{\rm SH}^{\rm ZnTe} = 70$ nm[88] is similar to that of $LuFe_2O_4$ ($l_{\rm SH} = 100$ nm [Sec. (2)]) hence the reflected SH can be measured using the same experimental setup [Fig. S1] and be compared. The phase mismatch effect is negligible therein, since $l_{\rm SH}^{\rm ZnTe}$ is shorter than the coherence length of the SH generation 164 nm, as well as $LuFe_2O_4$ [Sec. (2)]. The SH intensity of (110) ZnTe (||[001]) was 1.0×10^3 times stronger than that of $LuFe_2O_4$ ($\|a$), at the incident angles where the intensities show maximals. They are known to be proportional to $(d_{14}^{\rm ZnTe}/2)^2$ for ZnTe[87] and $(d_{11})^2$ for $LuFe_2O_4$ [Eq. (S2)]. Considering the difference in the penetration depths, namely, the active volumes for the SH generation, and in the reflection losses of the fundamental lights, we obtain the ra-

tio $d_{14}^{\mathrm{ZnTe}} : d_{11}^{\mathrm{LFO}} = 104 : 1$. Since $d_{14}^{\mathrm{ZnTe}} = 250\,\mathrm{pm/V}$ for the current wavelength[89], we estimate $d_{11}^{\mathrm{LFO}} = 2.4\,\mathrm{pm/V}$.

(4) TERAHERTZ-INDUCED DYNAMICS OF SHG ANISOTROPY

Figure S3 shows the polarization dependences of the transient SHG, upon applying b-polarized E_{THz}. The left-hand side presents the same $I_{\mathrm{SH}\|b}$ data as in Fig. 3, while explicitly showing time profiles at $\theta = 0°$ (blue diamonds) and 90° (green squares). Although the SHG at $\theta = 90°$ is forbidden in the steady state or $t \lesssim 0\,\mathrm{ps}$, it is activated at $t \simeq 0.7\,\mathrm{ps}$ near the maximum of E_{THz} to become comparably large with the allowed components ($\theta = 45°$ or 135°), unlike another SHG-forbidden component at $\theta = 0°$ which stayed almost zero. These contrastive changes clearly indicate the emergence of new symmetry by the E_{THz} breaking the ac mirror plane through tilting $\boldsymbol{P}$ out of it [Fig. 2], as described in the main text. On the other hand, it is hard to deduce its canting angle from our SHG experiments because the vector $\boldsymbol{P}$ cannot be uniquely determined from the nonlinear tensor.

The right-hand side of Fig. S3 shows time evolutions for $I_{\mathrm{SH}\|a}$. As seen, the terahertz-induced change ΔI_{SH} is far smaller (~10%) than those for $I_{\mathrm{SH}\|b}$ [the left-hand side]; accordingly, the anisotropies shown in polar plots almost stay in the original cross-like shape. This indicates that SHG is efficiently modulated by the E_{THz} having the parallel polarization.

SHG is also efficiently modulated when fundamental light and E_{THz} have parallel polarization. As Fig. 4 shows, d_{21}^* is smaller by less than one third of d_{22}^*, despite the resemblance in other characteristics. As seen in the definition of d^* tensor (see main text), the larger d_{22}^* term is related to b ($\|E_{\mathrm{THz}}$)-polarization E_bE_b, while the smaller d_{21}^* to E_aE_a ($\perp E_{\mathrm{THz}}$).

(5) TERAHERTZ-INDUCED EFFECTS ON THE FUNDAMENTAL FREQUENCY PULSE

E_{THz} can alter the linear susceptibility or the polarization state of the fundamental pulse to induce changes in I_{SH} [90]. To characterize the effect, we have measured the change of the reflected fundamental pulse upon applying the b-polarized E_{THz} [Fig. S4(a)] using the same setup as the SHG experiment [Fig. S1]. Neither the reflectivity change ΔR nor the polarization rotation was identified as described below, indicating that they are not responsible for the observed I_{SH} change [Fig. 2]. The small ΔR indicates the comparably small changes in the penetration depth, the refractive index and the resultant coherence length for SHG (i.e., the phase matching condition) mentioned in the section (2); therefore their effects on I_{SH} would be negligibly small, too.

As shown in Fig. S4(b), the E_{THz}-induced reflectivity change, $\Delta R/R$, was as small as 0.1% or less irrespective of the incident polarization angle θ. Such small change should not play a dominant role in the observed large I_{SH} increase up to 170% [Fig. 2].

The polar plots in Fig. S4(c) show normalized intensities of the reflected pulse for $\theta = 0°$ as a function of the analyzer [Fig. S1] angle ϕ ($\phi = 0°$ and 90° correspond to the a- and b-axes, respectively, as well as θ), at the delay times t indicated by vertical broken lines. Reflecting the linear-polarized fundamental pulse, the intensity measured without E_{THz} (blue closed circles) has a $\cos^2\phi$ shape. Importantly, as seen in red open circles, the E_{THz}-induced change is not identified even by the field stronger than 260 kV/cm which causes the +170% increase in I_{SH} [Fig. 2]. We have confirmed the same behavior at other delays ($-1.4\,\mathrm{ps} < t < 2.6\,\mathrm{ps}$, in time steps of 0.05 ps). The same holds for the cases of $\theta = 45°$[(d)] and 90°[(e)].

(6) FITTING ANALYSIS OF THE SHG ANISOTROPY

As described in the main text, $I_{\mathrm{SH}\|b}$ (I_{SH} hereafter) shown in Eq. (S3) will be modified by applying $E_{\mathrm{THz}}\|b$ breaking the ac mirror plane, to become

$$I_{\mathrm{SH}}(\theta) = (2d_{26}^* \sin\theta\cos\theta + d_{21}^* \cos^2\theta + d_{22}^* \sin^2\theta)^2, \quad \text{(S4)}$$

for the single domain case. $I_{\mathrm{SH}}(\theta)$ calculated for various d_{21}^* and d_{22}^* (normalized by d_{26}^*) are shown in Fig. S5. With activating d_{21}^* or d_{22}^*, the 4-fold symmetry in the steady state (i.e., $d_{21}^* = d_{22}^* = 0$) is broken to become anisotropic. reflecting the resultant lowest P1 symmetry. The distinctive shapes therein allow our fitting analysis to converge well, as seen in excellent overwrap against experimental data shown in Fig. 3(c), as well as small error bars (i.e., standard deviations of the least-square method) shown in Figs. 4(b)-(d). Some pieces of the crystal showed the anisotropy which is far from those in Fig. S5 and accordingly the fitting fails although Eq. (S4) is based on the lowest symmetry $P1$; this may happen in the multi-domain state, as described in the next section.

We also have carefully chosen initial guess values for the fitting, to avoid unstable results. As described below, we first simply estimated d_{ij}^* values using representative data, then used them as the initial values for the fitting. It is easy to deduce some absolute values from the measurement:

$$|d_{21}^*| = \sqrt{I_{\mathrm{SH}}(180°)}, \quad \text{(S5)}$$

$$|d_{22}^*| = \sqrt{I_{\mathrm{SH}}(90°)}. \quad \text{(S6)}$$

To obtain their signs, the following symmetric and antisymmetric terms can be used:

$$\frac{I_{\mathrm{SH}}(45°) - I_{\mathrm{SH}}(135°)}{2} = d_{26}^*(d_{21}^* + d_{22}^*),$$

$$\frac{I_{\mathrm{SH}}(45°+\alpha) - I_{\mathrm{SH}}(45°-\alpha) + I_{\mathrm{SH}}(135°+\alpha) - I_{\mathrm{SH}}(135°-\alpha)}{2} \times \frac{1}{\sin 4\alpha} = d_{26}^*(d_{21}^* - d_{22}^*),$$

yielding $d_{26}^*d_{21}^*$ and $d_{26}^*d_{22}^*$ by taking their sum and difference (we used $\alpha = 10°$). Consequently, we obtain signs of d_{21}^*

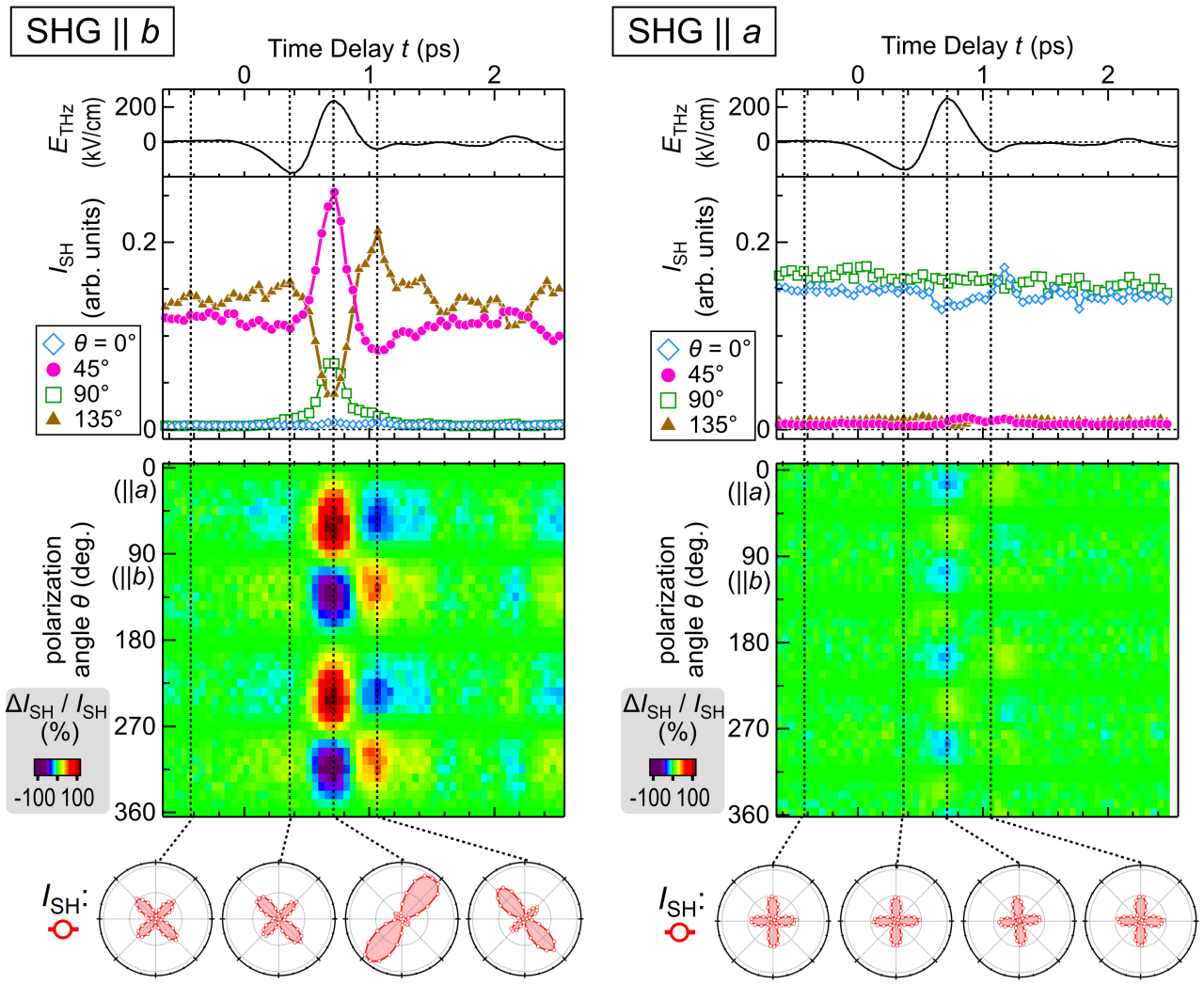

FIG. S3. Polarization dependence of transient SHG, upon applying E_{THz} along the b axis of $LuFe_2O_4$. $I_{\mathrm{SH}\|b}$ and $I_{\mathrm{SH}\|a}$ are shown in the left- and right-hand sides, respectively. The data for $I_{\mathrm{SH}\|b}$ are the same as those shown in Fig. 3. Top panels show waveforms of the E_{THz}. Right below, time profiles of E_{THz}-induced I_{SH} are shown for several fundamental angles, θ. Colormaps below show the change of $I_{\mathrm{SH}}(t,\theta)$, ΔI_{SH}, using ratio with respect to the maximal value in the steady state, $I_{\mathrm{SH}}(\theta = 45°)$. The data were measured in angle steps of 9°, and time steps of 0.05 ps. Polar plots below show anisotropies of $I_{\mathrm{SH}}(\theta)$ at several time delays indicated by broken lines.

and d^*_{22} (with respect to d^*_{26}), thus can derive them using the absolute values shown above. Since I_{SH} is unchanged by the inversion $d^* \to -d^*$, we may set d_{26} positive for the reference purpose. Finally, we note that sometimes the simple initial values $d_{26} = 1, d_{21} = d_{22} = 0$ yield the same results.

(7) ON THE POSSIBILITY OF A MULTIDOMAIN STATE

As shown in Fig. 3(c), the observed anisotropies of $I_{\mathrm{SH}\|b}$ (hereafter I_{SH}) are excellently reproduced by the tensor analysis or Eq. (S3) which is based on the single $\boldsymbol{P}$ domain. On the other hand, the analysis considering a multi-domain state with antiparallel $\boldsymbol{P}$ fails, as described below.

In general, a ferroelectric crystal comprises domains having antiparallel $\boldsymbol{P}$ [91], hence resultant nonlinear susceptibility d will be oppositely signed therein. The sign will not affect SHG intensity in the steady state; I_{SH} remains unchanged upon the sign change of d_{26} [Eq. (S3)]. In contrast, it would affect the terahertz-induced I_{SH} [Eq. (S4)]; it contains, in addition to d^*_{26} being odd against $\boldsymbol{P}$, d^*_{21} and d^*_{22} which are zero in the steady state but activated by E_{THz} irrespective of the sign of $\boldsymbol{P}$. In other words, the sign change of $\boldsymbol{P}$ only inverts the d^*_{26} term and hence its interference with the d^*_{21} and d^*_{22} terms may affect I_{SH}.

I_{SH} from the multi ($\pm\boldsymbol{P}$)-domains with equal volume frac-

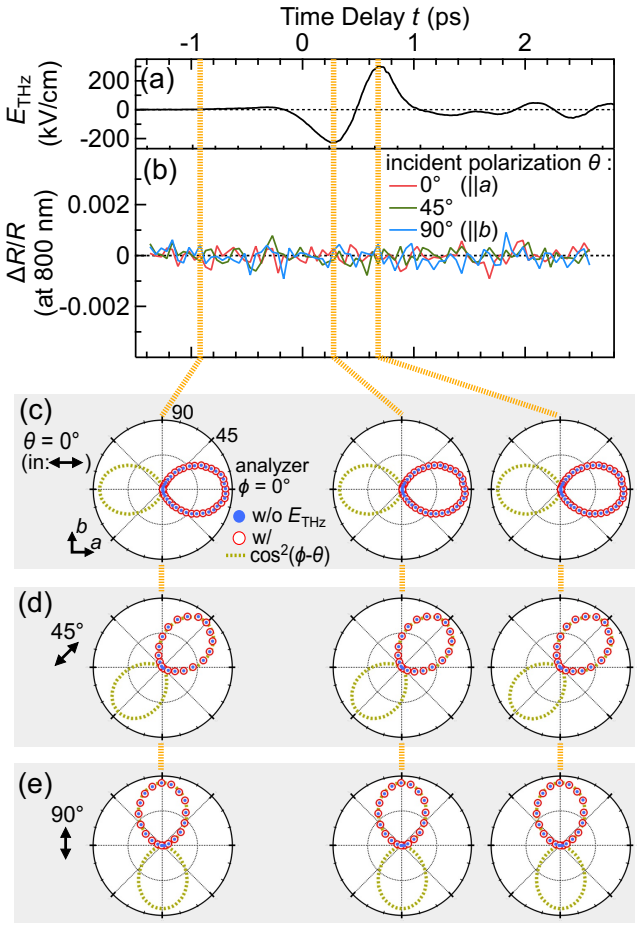

FIG. S4. Terahertz-induced effects on the FF pulse at 800 nm. (a) The E_{THz} waveform applied to the sample ($\|b$). (b) Terahertz-induced change in reflectivity with incident light polarizations $\theta = 0°, 45°, 90°$. (c)(d)(e) Normalized intensities of the reflected pulses with incident light polarizations $\theta = 0°, 45°, 90°$ as a function of the analyzer angle ϕ. Blue closed circles and red open circles represent intensities measured without and with E_{THz}, respectively. Green dotted lines represent $\cos^2(\phi - \theta)$.

tion will be

$$I_{\mathrm{SH}}^{(+)} + I_{\mathrm{SH}}^{(-)} =$$
$$(\,2d_{26}^{*}\sin\theta\cos\theta + d_{21}^{*}\cos^2\theta + d_{22}^{*}\sin^2\theta)^2$$
$$+(-2d_{26}^{*}\sin\theta\cos\theta + d_{21}^{*}\cos^2\theta + d_{22}^{*}\sin^2\theta)^2$$
$$= \left(d_{21}^{*}\cos^2\theta + d_{22}^{*}\sin^2\theta\right)^2 + 4{d_{26}^{*}}^2\sin^2\theta\cos^2\theta. \qquad \text{(S7)}$$

As seen, it is symmetric against the inversion of θ, i.e., the corresponding polar plot should show a vertically-symmetric shape, which is far from the observations [lower-left of Fig. 2 and Fig. 3(c)]. Therefore, our results are reasonably ascribed to the response of the single domain. Since the E_{THz} used therein is b-polarized or perpendicular to $\boldsymbol{P}$, it should not modulate the ferroelectric domain distribution nor should give rise to the multi-domain state.

The data shown in this paper were obtained by irradiating

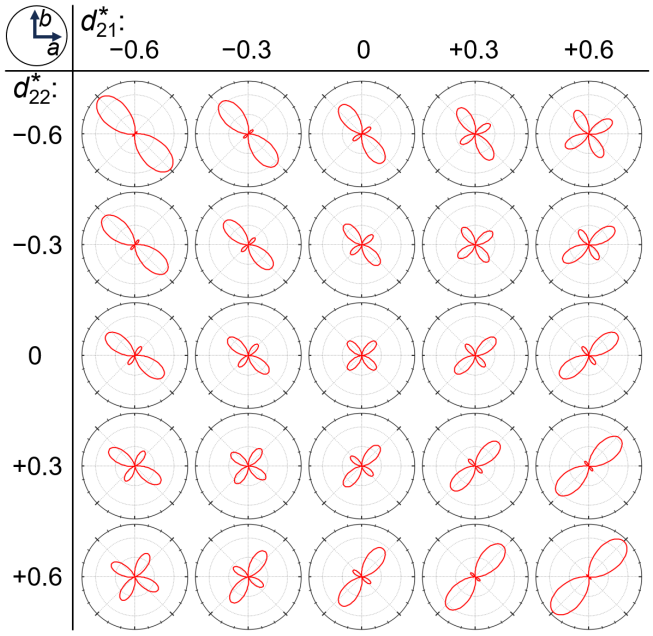

FIG. S5. $I_{\mathrm{SH}}(\theta)$ for various d_{21}^{*} and d_{22}^{*}.

a specific position of the sample with the incident light having a spot size of 300 μm. Although a multi-domain state is unlikely therein as discussed above, it should be noted that it is far larger than those of CO domains previously reported, which are less than 1 μm[34, 71, 92–97]. We believe that such a large coherence in $\boldsymbol{P}$ has been realized thanks to the recent improvement in crystal quality in our stoichiometric sample[81]. Note that our experiments cannot determine the absolute sign of d^{*} or $\boldsymbol{P}$. In order to resolve its spatial distribution, other experiments, such as terahertz generation, are required[82, 98].

(8) ANALYSIS BASED ON THIRD-ORDER NONLINEAR SUSCEPTIBILITY

SHG intensity I and its modulation by an external electric field E^{ex} are usually analyzed by 2nd- and 3rd-order susceptibilities: $\chi^{(2)}$and $\chi^{(3)}$. While the observed SHG anisotropy is well reproduced by them, its field-induced dynamics cannot be explained by the inherent $\chi^{(3)}$; the derived $\chi^{(3)}$unusually increased by an order of magnitude within 1 picosecond, as shown below.

With near-infrared fundamental light E^{ω} ($\hbar\omega \approx 1.55$ eV), SHG intensity is expressed as

$$I_i \propto \left(\sum_{jk}\chi_{ijk}^{(2)}(2\omega;\omega,\omega)E_j^{\omega}E_k^{\omega} + \sum_{jkl}\chi_{ijkl}^{(3)}(2\omega;\omega,\omega,0)E_j^{\omega}E_k^{\omega}E_l^{\mathrm{ex}}\right)^2 \qquad \text{(S8)}$$

where i, j, k, l represent crystallographic axes. THz electric field E_{THz} can be regarded as E^{ex} since $\omega_{\mathrm{THz}} \ll \omega$; this terahertz field-induced second harmonic (referred to as TFISH)

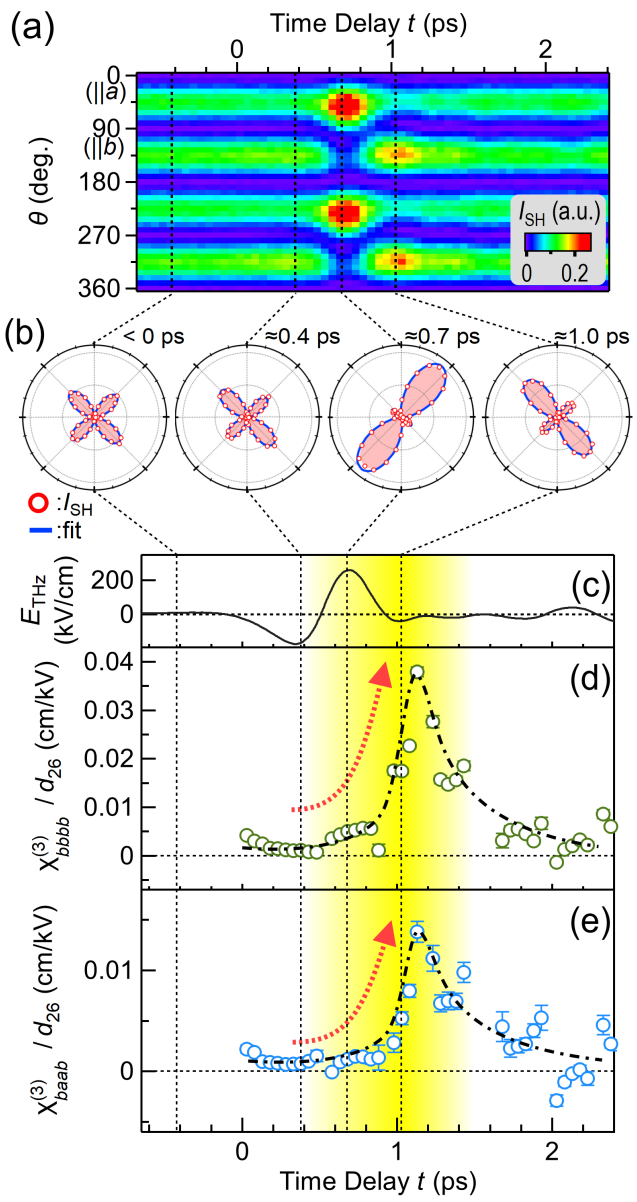

FIG. S6. Time evolutions of SHG ($\|b$) anisotropy. (a) Dataset of $I_{SH}(\theta)$ at each time delay. (b) Polar plots of $I_{SH}(\theta)$ (red circles) at delays indicated by vertical lines in (a) and (c)-(e). Blue solid lines show fitting curves. (c) E_{THz} ($\|b$) waveform applied to the sample. (d)(e) $\chi^{(3)}_{bbbb}$ and $\chi^{(3)}_{baab}$ derived by the fitting using Eq. (S9). Error bars, which are as small as marker circles, represent standard deviations of the fitting. At delays where $E_{THz} \approx 0$, the estimated $\chi^{(3)}$ may be inaccurate because the normalization of small $\Delta I_{SH\|b}$ by small E_{THz} is seriously sensitive to any experimental errors; such results therein are not shown.

has explained various dynamics of SHG intensity [99–101]. Among $\chi^{(2)}_{ijk}$ and $\chi^{(3)}_{ijkl}$ components, many are zero due to the symmetry of the used single crystal [87] belonging to monoclinic Cm with the mirror plane perpendicular to the b axis [Fig. 1]. A more limited number of components contribute to the present observation, i.e. measuring $I_{SH\|b}$ from the ab-plane using fundamental light $(E_a, E_b) = E_0(\cos\theta, \sin\theta)$ ($\theta = 0°$ corresponds to the a-axis) and $E_{THz}\|b$, hence Eq. (S8) is rewritten as

$$I_{SH\|b}(\theta) \propto (4d_{26}\sin\theta\cos\theta + \chi^{(3)}_{baab}\cos^2\theta E_{THz} + \chi^{(3)}_{bbbb}\sin^2\theta E_{THz})^2, \quad \text{(S9)}$$

where $d_{26} \equiv \frac{1}{2}\chi^{(2)}_{bab} = \frac{1}{2}\chi^{(2)}_{bba}$. Through the fitting analysis of the observed anisotropy $I_{SH\|b}(\theta)$ shown in Fig. S6(a), one can derive d_{26} and $\chi^{(3)}$from the data without and with E_{THz}, respectively. Note that θ-dependence of Eq. (S9) is similar to that for the analysis given in the main text [Eq. (2)];

$$I_{SH\|b}(\theta) \propto \left(2d^*_{26}\sin\theta\cos\theta + d^*_{21}\cos^2\theta + d^*_{22}\sin^2\theta\right)^2, \quad \text{(S10)}$$

where d^* represent the modulated tensor components. Since $d^*_{26} \approx d_{26}$ [Fig. 4(d)], d^*_{21} and d^*_{22} shown in Figs. 4(b) and (c) roughly correspond to $\chi^{(3)}_{baab}E_{THz}$ and $\chi^{(3)}_{bbbb}E_{THz}$, respectively.

The result of the fitting using Eq. (S9) is shown in Figs. S6(b)-(e). In panel (b) we show polar plots of the observed $I_{SH\|b}(\theta)$ (red circles) and the fitting curves (blue solid lines) at the delays indicated by the vertical lines in (c)-(e) where E_{THz}, derived $\chi^{(3)}_{baab}$ and $\chi^{(3)}_{bbbb}$ are shown. As shown in (b), the fitting showed good agreement with the observed anisotropy like Fig. 3(c).

It should be noted, however, that the observed time evolution cannot be reproduced by the inherent $\chi^{(3)}_{baab}$ or $\chi^{(3)}_{bbbb}$. As shown in (d), $\chi^{(3)}_{bbbb}$ stays as small as ≈ 0.001 (the value, being normalized by d_{26}, is in unit of cm/kV) at $t \simeq 0.4$ ps where E_{THz} has the largest negative value. Thereafter, it increases to ≈ 0.005 at $t \simeq 0.7$ ps upon the maximum E_{THz}, and even to ≈ 0.02 or larger at $t \approx 1.0$ ps. This unusual one-order-of-magnitude increase is also seen in $\chi^{(3)}_{baab}$ [(e)], both of which are far larger than standard deviations of the fitting represented by error bars (many of them are smaller than markers). The behavior reflects $I_{SH\|b}(45°)$ [Fig. 3(a)] or d^* [Figs. 4 and 5] showing the terahertz-induced change which is more significant at $t \approx 1.0$ ps than at $t \approx 0.4$ ps despite that $|E_{THz}(1.0\,\text{ps})| < |E_{THz}(0.4\,\text{ps})|$. Such dynamics cannot be ascribed to a mere nonlinearity against E_{THz}. At $t \geq 1.0$ ps $\chi^{(3)}$gets smaller, showing qualitative agreement with the time profile of the sensitivity K shown in Fig. 5.

Our observation has been confirmed to accompany unusual increase of the nonlinear susceptibilities irrespective of their order. As the most plausible physical picture for this, we understood it as the ultrafast response of ferroelectric polarization or the resultant d^* and the concomitant cooperative effect. It may be difficult to give a particular physical scenario to the modulation in $\chi^{(3)}$at the cost of its generality.

(9) TRANSIENT SENSITIVITY

One way to represent terahertz-induced dynamics is a parametric plot; the target quantity is plotted against E_{THz}

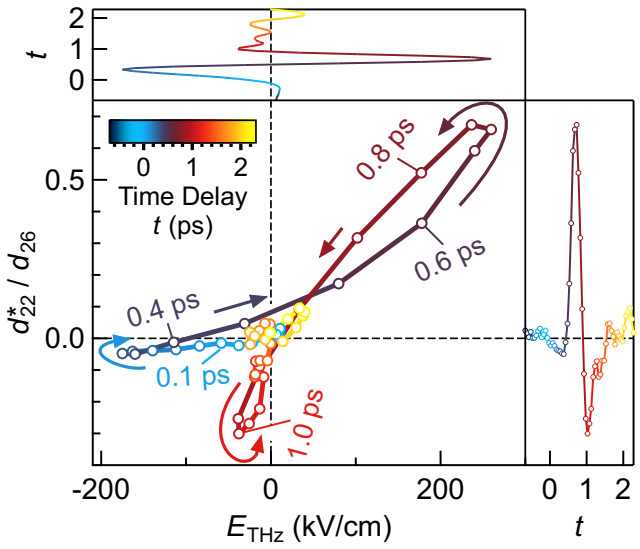

FIG. S7. Parametric plot of d^* as a function of E_{THz}. d^*_{22}/d_{26} is plotted against E_{THz} values at the same t. Its time evolution is represented by color.

value, thus its sensitivity corresponds to the slope therein. Those in preceding studies can be characterized by a linear shape[100, 102–104], indicating that the sensitivity stays almost constant during the application of E_{THz}, although the sign of the slope sometimes inverts if the quantity is an even function of E_{THz}.

The parametric plot of d^*_{22} shown in Fig. S7, which uses the same data as in Fig. 5, is not like that; while it is almost horizontal at the beginning (cyan, ≃0 ps), it becomes steeper with time (brown, ≃0.7 ps) to be nearly vertical (orange, ≃1 ps). The increase in the slope corresponds to that for the sensitivity [Fig. 5(b)].

* hri@kwansei.ac.jp; Present address: Department of Physics and Astronomy, Kwansei Gakuin University, Sanda 669-1330, Japan.
† Present address: National Institutes for Quantum and Radiological Science and Technology, Sayo 679-5148, Japan
‡ okimoto.y.aa@m.titech.ac.jp
§ s-iwai@tohoku.ac.jp

[1] S. Ishihara, J. Phys. Soc. Jpn. **79**, 011010 (2010).
[2] M. Angst, Phys. Stat. Sol. (RRL) **7**, 383 (2013).
[3] N. Ikeda, T. Nagata, J. Kano, and S. Mori, J. Phys.: Condens. Matter **27**, 053201 (2015).
[4] T. Nagata, Mater. Sci. Eng. Int. J. **2**, 35 (2018).
[5] N. Tannières, O. Évrard, and J. Aubry, C. R. Acad. Sc. (Paris) **278C**, 241 (1974).
[6] O. Évrard, B. Malaman, F. Jeannot, N. Tannières, and J. Aubry, C. R. Acad. Sc. (Paris) **278C**, 413 (1974).
[7] N. Kimizuka, A. Takenaka, Y. Sasada, and T. Katsura, Solid State Commun. **15**, 1199 (1974).
[8] N. Kimizuka, A. Takenaka, Y. Sasada, and T. Katsura, Solid State Commun. **15**, 1321 (1974).
[9] E. J. W. Verwey, Nature **144**, 327 (1939).
[10] M. Tanaka, K. Siratori, and N. Kimizuka, J. Phys. Soc. Jpn. **53**, 760 (1984).
[11] M. Tanaka, H. Iwasaki, K. Siratori, and I. Shindo, J. Phys. Soc. Jpn. **58**, 1433 (1989).
[12] J. Iida, M. Tanaka, Y. Nakagawa, S. Funahashi, N. Kimizuka, and S. Takekawa, J. Phys. Soc. Jpn. **62**, 1723 (1993).
[13] Y. Yamada, S. Nohdo, and N. Ikeda, J. Phys. Soc. Jpn. **66**, 3733 (1997).
[14] Y. Yamada, K. Kitsuda, S. Nohdo, and N. Ikeda, Phys. Rev. B **62**, 12167 (2000).
[15] N. Ikeda, K. Saito, K. Kohn, H. Kito, J. Akimitsu, and K. Siratori, Ferroelectrics **161**, 111 (1994).
[16] N. Ikeda, K. Kohn, H. Kito, J. Akimitsu, and K. Siratori, J. Phys. Soc. Jpn. **64**, 1371 (1995).
[17] N. Ikeda, K. Kohn, N. Myouga, E. Takahashi, H. Kitôh, and S. Takekawa, J. Phys. Soc. Jpn. **69**, 1526 (2000).
[18] N. Ikeda, H. Ohsumi, K. Ohwada, K. Ishii, T. Inami, K. Kakurai, Y. Murakami, K. Yoshii, S. Mori, Y. Horibe, and H. Kitô, Nature **436**, 1136 (2005).
[19] J. van den Brink and D. I. Khomskii, J. Phys.: Condens. Matter **20**, 434217 (2008).
[20] M. A. Subramanian, T. He, J. Chen, N. S. Rogado, T. G. Calvarese, and A. W. Sleight, Adv. Mater. **18**, 1737 (2006).
[21] J. Y. Park, J. H. Park, Y. K. Jeong, and H. M. Jang, Appl. Phys. Lett. **91**, 152903 (2007).
[22] C. R. Serrao, J. R. Sahu, K. Ramesha, and C. N. R. Rao, J. Appl. Phys. **104**, 016102 (2008).
[23] H. Yang, H. Tian, Y. Zhang, Y. Qin, L. Zeng, C. Ma, H. Shi, and J. Lu, Solid State Commun. **150**, 1467 (2010).
[24] J. Rouquette, J. Haines, A. Al-Zein, P. Papet, F. Damay, J. Bourgeois, T. Hammouda, F. Doré, A. Maignan, M. Hervieu, and C. Martin, Phys. Rev. Lett. **105**, 237203 (2010).
[25] A. M. Mulders, M. Bartkowiak, J. R. Hester, E. Pomjakushina, and K. Conder, Phys. Rev. B **84**, 140403(R) (2011).
[26] D. Ohishi, H. Hayakawa, H. Akahama, N. Ikeda, T. Kambe, Y. Matsuo, N. Kimizuka, J. Kano, and K. Yoshii, Ferroelectrics **415**, 51 (2011).
[27] A. Ruff, S. Krohns, F. Schrettle, V. Tsurkan, P. Lunkenheimer, and A. Loidl, Eur. Phys. J. B **85**, 290 (2012).
[28] D. Niermann, F. Waschkowski, J. de Groot, M. Angst, and J. Hemberger, Phys. Rev. Lett. **109**, 016405 (2012).
[29] J. de Groot, T. Mueller, R. A. Rosenberg, D. J. Keavney, Z. Islam, J.-W. Kim, and M. Angst, Phys. Rev. Lett. **108**, 187601 (2012).
[30] A. J. Hearmon, D. Prabhakaran, H. Nowell, F. Fabrizi, M. J. Gutmann, and P. G. Radaelli, Phys. Rev. B **85**, 014115 (2012).
[31] J. Bourgeois, M. Hervieu, M. Poienar, A. M. Abakumov, E. Elkaïm, M. T. Sougrati, F. Porcher, F. Damay, J. Rouquette, G. V. Tendeloo, A. Maignan, J. Haines, and C. Martin, Phys. Rev. B **85**, 064102 (2012).
[32] Y. Sun, Y. Liu, F. Ye, S. Chi, Y. Ren, T. Zou, F. Wang, and L. Yan, J. Appl. Phys. **111**, 07D902 (2012).
[33] T. Kambe, Y. Fukada, J. Kano, T. Nagata, H. Okazaki, T. Yokoya, S. Wakimoto, K. Kakurai, and N. Ikeda, Phys. Rev. Lett. **110**, 117602 (2013).
[34] I. K. Yang, J. Kim, S. H. Lee, S.-W. Cheong, and Y. H. Jeong, Appl. Phys. Lett. **106**, 152902 (2015).
[35] L. J. Zeng, H. X. Yang, Y. Zhang, H. F. Tian, C. Ma, Y. B. Qin, Y. G. Zhao, and J. Q. Li, Europhys. Lett. **84**, 57011 (2008).
[36] C.-H. Li, X.-Q. Zhang, Z.-H. Cheng, and Y. Sun, Appl. Phys. Lett. **92**, 182903 (2008).

[37] C. Li, X. Zhang, Z. Cheng, and Y. Sun, Appl. Phys. Lett. **93**, 152103 (2008).
[38] C.-H. Li, F. Wang, Y. Liu, X.-Q. Zhang, Z.-H. Cheng, and Y. Sun, Phys. Rev. B **79**, 172412 (2009).
[39] J. Wen, G. Xu, G. Gu, and S. M. Shapiro, Phys. Rev. B **80**, 020403(R) (2009).
[40] Y. Liu, T. Zou, F. Wang, X.-Q. Zhang, Z.-H. Cheng, and Y. Sun, Physica B **405**, 3391 (2010).
[41] F. Wang, C.-H. Li, T. Zou, Y. Liu, and Y. Sun, J. Phys.: Condens. Matter **22**, 496001 (2010).
[42] N. Ikeda, M. Kubota, H. Hayakawa, H. Akahama, D. Ohishi, A. Nakanishi, T. Funabiki, Y. Matsuo, N. Kimizuka, T. Kambe, S. Mori, and J. Kano, Ferroelectrics **414**, 41 (2011).
[43] J. Wen, G. Xu, G. Gu, and S. M. Shapiro, Phys. Rev. B **81**, 144121 (2010).
[44] X. Xu, K. Seal, X. Xu, I. Ivanov, C.-H. Hsueh, N. A. Hatab, L. Yin, X. Zhang, Z. Cheng, B. Gu, Z. Zhang, and J. Shen, Nano Lett. **11**, 1265 (2011).
[45] B. Fisher, J. Genossar, L. Patlagan, and G. M. Reisner, J. Appl. Phys. **109**, 084111 (2011).
[46] S. Cao, J. Li, H. F. Tian, Y. B. Qin, L. J. Zeng, H. X. Yang, and J. Q. Li, Appl. Phys. Lett. **98**, 102102 (2011).
[47] F. Wang, T. Zou, Y. Liu, L.-Q. Yan, and Y. Sun, J. Appl. Phys. **111**, 033703 (2012).
[48] K. Fujiwara, T. Hori, and H. Tanaka, J. Phys. D: Appl. Phys. **46**, 155108 (2013).
[49] T. Nagata, Y. Fukada, M. Kawai, J. Kano, T. Kambe, E. Dudzik, R. Feyerherm, P. E. Janolin, J. M. Kiat, and N. Ikeda, Ferroelectrics **442**, 45 (2013).
[50] K. Yoshii, D. Matsumura, H. Saitoh, T. Kambe, M. Fukunaga, Y. Muraoka, N. Ikeda, and S. Mori, J. Phys. Soc. Jpn. **83**, 063708 (2014).
[51] S. Z. Li, S. J. Luo, R. Fu, B. B. Jin, K. F. Wang, ·. M. Liu, J. F. Ding, and X. G. Li, Appl. Phys. A **96**, 893 (2009).
[52] X. S. Xu, J. de Groot, Q.-C. Sun, B. C. Sales, D. Mandrus, M. Angst, A. P. Litvinchuk, and J. L. Musfeldt, Phys. Rev. B **82**, 014304 (2010).
[53] R. Wang, H. X. Yang, Y. B. Qin, B. Dong, J. Q. Li, and J. Zhao, J. Appl. Phys. **108**, 073507 (2010).
[54] F. M. Vitucci, A. Nucara, D. Nicoletti, Y. Sun, C. H. Li, J. C. Soret, U. Schade, and P. Calvani, Phys. Rev. B **81**, 195121 (2010).
[55] C. Lee, J. Kim, S. W. Cheong, and E. J. Choi, Phys. Rev. B **85**, 014303 (2012).
[56] A. Glamazda, K.-Y. Choi, P. Lemmens, D. Wulferding, S. Park, and S.-W. Cheong, Phys. Rev. B **87**, 144416 (2013).
[57] J. Lee, S. A. Trugman, C. D. Batista, C. L. Zhang, D. Talbayev, X. S. Xu, S.-W. Cheong, D. A. Yarotski, A. J. Taylor, and R. P. Prasankumar, Sci. Rep. **3**, 2654 (2013).
[58] H. Itoh, K. Itoh, K. Anjyo, H. Nakaya, H. Akahama, D. Ohishi, S. Saito, T. Kambe, S. Ishihara, N. Ikeda, and S. Iwai, J. Lumin. **133**, 149 (2013).
[59] J. Lee, S. A. Trugman, C. L. Zhang, D. Talbayev, X. S. Xu, S.-W. Cheong, D. A. Yarotski, A. J. Taylor, and R. P. Prasankumar, Appl. Phys. Lett. **107**, 042906 (2015).
[60] X. Liu, Z. Jin, Z. Cheng, X. Lin, G. Balakrishnan, and G. Ma, Phys. Stat. Sol. (RRL) **11**, 1700177 (2017).
[61] A. Nagano, M. Naka, J. Nasu, and S. Ishihara, Phys. Rev. Lett. **99**, 217202 (2007).
[62] A. Nagano and S. Ishihara, J. Phys.: Condens. Matter **19**, 145263 (2007).
[63] H. J. Xiang and M.-H. Whangbo, Phys. Rev. Lett. **98**, 246403 (2007).
[64] J. Nasu, A. Nagano, M. Naka, and S. Ishihara, Phys. Rev. B **78**, 024416 (2008).
[65] M. Naka, A. Nagano, and S. Ishihara, Phys. Rev. B **77**, 224441 (2008).
[66] T. Watanabe and S. Ishihara, J. Phys. Soc. Jpn. **78**, 113702 (2009).
[67] T. Watanabe and S. Ishihara, J. Phys. Soc. Jpn. **79**, 114714 (2010).
[68] A. B. Harris and T. Yildirim, Phys. Rev. B **81**, 134417 (2010).
[69] Y. B. Kudasov and D. A. Maslov, Phys. Rev. B **86**, 214427 (2012).
[70] M. Iwata and Y. Ishibashi, J. Phys. Soc. Jpn. **81**, 035003 (2012).
[71] S. Mori, S. Shinohara, Y. Matsuo, Y. Horibe, K. Yoshii, and N. Ikeda, Jpn. J. Appl. Phys. **47**, 7595 (2008).
[72] T. Michiuchi, Y. Yokota, T. Komatsu, H. Hayakawa, T. Kuroda, D. Maeda, Y. Matsuo, S. Mori, K. Yoshii, N. Hanasaki, T. Kambe, and N. Ikeda, Ferroelectrics **378**, 175 (2010).
[73] M. Hervieu, A. Guesdon, J. Bourgeois, E. Elkaïm, M. Poienar, F. Damay, J. Rouquette, A. Maignan, and C. Martin, Nature Mater. **13**, 74 (2014).
[74] T. Mueller, J. de Groot, J. Strempfer, and M. Angst, J. Cryst. Growth **428**, 40 (2015).
[75] K. Fujiwara, M. Miyajima, M. Fukunaga, J. Kano, H. Kobayashi, and N. Ikeda, Trans. Mater. Res. Soc. Jpn. **41**, 139 (2016).
[76] P. Ren, Z. Yang, W. G. Zhu, C. H. A. Huan, and L. Wang, J. Appl. Phys. **109**, 074109 (2011).
[77] K. Fujiwara, T. Karasudani, K. Kakurai, W. T. Lee, K. C. Rule, A. J. Studer, and N. Ikeda, J. Phys. Soc. Jpn. **88**, 044701 (2019).
[78] T. Nagata, P.-E. Janolin, M. Fukunaga, B. Roman, K. Fujiwara, H. Kimura, J.-M. Kiat, and N. Ikeda, Appl. Phys. Lett. **110**, 052901 (2017).
[79] K. Fujiwara, T. Karasudani, M. Fukunaga, H. Kobayashi, J. Kano, P.-E. Janolin, J.-M. Kiat, Y. Nogami, R. Kondo, and N. Ikeda, Ferroelectrics **512**, 85 (2017).
[80] M. Angst, R. P. Hermann, A. D. Christianson, M. D. Lumsden, C. Lee, M.-H. Whangbo, J.-W. Kim, P. J. Ryan, S. E. Nagler, W. Tian, R. Jin, B. C. Sales, and D. Mandrus, Phys. Rev. Lett. **101**, 227601 (2008).
[81] K. Fujiwara, Y. Fukada, Y. Okuda, R. Seimiya, N. Ikeda, K. Yokoyama, H. Yu, S. Koshihara, and Y. Okimoto, Sci. Rep. **11**, 4277 (2021).
[82] H. Yu, Y. Okimoto, A. Morita, S. Shimanuki, K. Takubo, T. Ishikawa, S. Koshihara, R. Minakami, H. Itoh, S. Iwai, N. Ikeda, T. Sakagami, M. Nozaki, and T. Fujii, Materials **16**, 1989 (2023).
[83] H. Yu, Y. Fukada, G. Nishida, K. Takubo, T. Ishikawa, S. Koshihara, N. Ikeda, and Y. Okimoto, Phys. Rev. Mater. **8**, 064402 (2024).
[84] S. Konishi, D. Urushihara, T. Hayakawa, K. Fukuda, T. Asaka, K. Ishii, N. Naoda, M. Okada, H. Akamatsu, H. Hojo, M. Azuma, and K. Tanaka, Phys. Rev. B **108**, 014105 (2023).
[85] J. Hebling, G. Almasi, I. Kozma, and J. Kuhl, Opt. Express **10**, 1161 (2002).
[86] H. Hirori, A. Doi, F. Blanchard, and K. Tanaka, Appl. Phys. Lett. **98**, 091106 (2011).
[87] R. W. Boyd, *Nonlinear Optics (3rd Edition)* (Academic Press, 2008).
[88] K. Sato and S. Adachi, J. Appl. Phys. **73**, 926 (1993).
[89] H. P. Wagner, M. Kühnelt, W. Langbein, and J. M. Hvam, Phys. Rev. B **58**, 10494 (1998).
[90] M. Cornet, J. Degert, E. Abraham, and E. Freysz, Opt. Lett.

39, 5921 (2014).
[91] A. K. Tagantsev, L. E. Cross, and J. Fousek, *Domains in Ferroic Crystals and Thin Films* (Springer, 2010).
[92] Y. Murakami, N. Abe, T. Arima, and D. Shindo, Phys. Rev. B **76**, 024109 (2007).
[93] S. Park, Y. Horibe, Y. J. Choi, C. L. Zhang, S.-W. Cheong, and W. Wu, Phys. Rev. B **79**, 180401(R) (2009).
[94] Y. Zhang, H. X. Yang, Y. Q. Guo, C. Ma, H. F. Tian, J. L. Luo, and J. Q. Li, Phys. Rev. B **76**, 184105 (2007).
[95] Y. Zhang, H. X. Yang, C. Ma, H. F. Tian, and J. Q. Li, Phys. Rev. Lett. **98**, 247602 (2007).
[96] T. Maruyama, Y. Murakami, D. Shindo, N. Abe, and T. Arima, Phys. Rev. B **86**, 054202 (2012).
[97] Y. Horibe, S. Mori, N. Ikeda, K. Yoshii, H. Maeno, and Y. Murakami, Ferroelectrics **584**, 20 (2021).
[98] H. Itoh, H. Obatake, R. Fujiwara, Y. Kawakami, K. Yamamoto, M. Dressel, and S. Iwai, Phys. Rev. Research **3**, L032043 (2021).
[99] F. Chen, J. Goodfellow, S. Liu, I. Grinberg, M. C. Hoffmann, A. R. Damodaran, Y. Zhu, P. Zalden, X. Zhang, I. Takeuchi, A. M. Rappe, L. W. Martin, H. Wen, and A. M. Lindenberg, Adv. Mater. **27**, 6371 (2015).
[100] K. A. Grishunin, N. A. Ilyin, N. E. Sherstyuk, E. D. Mishina, A. Kimel, V. M. Mukhortov, A. V. Ovchinnikov, O. V. Chefonov, and M. B. Agranat, Sci. Rep. **7**, 687 (2017).
[101] K. Grishunin, V. Bilyk, N. Sherstyuk, V. Mukhortov, A. Ovchinnikov, O. Chefonov, M. Agranat, E. Mishina, and A. V. Kimel, Sci. Rep. **9**, 697 (2019).
[102] T. Miyamoto, H. Yada, H. Yamakawa, and H. Okamoto, Nature Commun. **4**, 2586 (2013).
[103] T. Miyamoto, D. Hata, T. Morimoto, H. Yamakawa, N. Kida, T. Terashige, K. Iwano, H. Kishida, S. Horiuchi, and H. Okamoto, Sci. Rep. **8**, 15014 (2018).
[104] T. Umanodan, K. Kaneshima, K. Takeuchi, N. Ishii, J. Itatani, H. Hirori, Y. Sanari, K. Tanaka, Y. Kanemitsu, T. Ishikawa, S. Koshihara, S. Horiuchi, and Y. Okimoto, J. Phys. Soc. Jpn. **88**, 013705 (2019).